Influence of horizontal resolution and complexity of aerosol-cloud interactions on marine stratocumulus and stratocumulus-to-cumulus transition in HadGEM3-GC3.1

Received: 4 December 2022 | Revised: 27 April 2023 | Accepted: 16 May 2023

DOI: 10.1002/qj.4494

Quarterly Journal of the Royal Meteorological Society RMetS

RESEARCH ARTICLE

Influence of horizontal resolution and complexity of aerosol–cloud interactions on marine stratocumulus and stratocumulus-to-cumulus transition in HadGEM3-GC3.1

Annica M. L. Ekman[1] | **Eva Nygren**[1] | **Alejandro Baró Pérez**[1] | **Matthias Schwarz**[1] | **Gunilla Svensson**[1] | **Nicolas Bellouin**[2]

[1]Department of Meteorology and Bolin Centre for Climate Research, Stockholm University, Stockholm, Sweden

[2]Department of Meteorology, University of Reading, Reading, UK

Correspondence
Annica M. L. Ekman, Department of Meteorology and Bolin Centre for Climate Research, Stockholm University, Stockholm, Sweden.
Email: annica@misu.su.se

Present address
Matthias Schwarz, Zentralanstalt für Meteorologie und Geodynamik – ZAMG, Vienna, Austria

Funding information
European Commission, Grant/Award Number: 641727 (PRIMAVERA)

Abstract

Stratocumulus (Sc) clouds and stratocumulus-to-cumulus transitions (SCTs) are challenging to represent in global models and they contribute to a large spread in modeled subtropical cloud feedbacks. We evaluate the impact of increasing the horizontal model resolution (~135, 60 and 25 km, respectively) and increasing the complexity of the aerosol–cloud interaction parameterization (interactive versus non-interactive at medium resolution) on springtime subtropical marine Sc properties and SCTs in the atmosphere-only version of HadGEM3-GC3.1. No significant impact on the spatial location of the SCT could be found between the different model versions. Increasing horizontal resolution led to small but significant increases in liquid water content and a stronger (more negative) shortwave (SW) cloud radiative effect (CRE), in particular over the southern-hemisphere Sc regions. However, for two out of the four studied regions, the stronger SW CRE also brought the model outside the range of satellite-derived values of the SW CRE. Applying non-interactive aerosols instead of interactive aerosols also led to significantly higher liquid water content and a stronger SW CRE over the southern-hemisphere Sc regions, while over the northern-hemisphere Sc regions, a competition between a substantial increase in the cloud droplet number concentration and small changes in the liquid water content resulted in a weaker SW CRE or non-significant changes. In general, using interactive instead of non-interactive aerosol–cloud interactions brought the model closer to satellite-retrieved mean values of the SW CRE. Our results suggest that increasing the horizontal resolution or the complexity of the aerosol–cloud parameterization has a small but statistically significant effect on the SW CRE of marine Sc, in particular over regions with high liquid water content. For these regions, the effect of introducing non-interactive versus interactive aerosol–cloud interactions is about as large as increasing the horizontal resolution from medium to high.

KEYWORDS

aerosol–cloud interaction, general circulation model, stratocumulus, stratocumulus-to-cumulus transition

1 | INTRODUCTION

Marine stratocumuli (Sc) cover 20%–25% of the world's oceans and are globally the dominant cloud type in terms of their areal extent (Norris, 1998; Wood, 2012). They have a strong negative global average radiative effect, and a small change in the fraction of marine Sc may substantially impact global climate (Slingo, 1990). Conditions for marine Sc formation are favorable over the cold parts of the subtropical and tropical oceans, within the subsidence regions along the eastern boundaries of the large ocean basins (Wood, 2012). Trade winds advect the marine Sc westward and toward the equator where they eventually break up into trade wind cumuli, so-called stratocumulus-to-cumulus transitions (SCTs; Albrecht *et al.*, 1995; Bretherton and Wyant, 1997; Wood and Bretherton, 2004; Sandu and Stevens, 2011). SCTs are mainly driven by an increase in sea surface temperature (Bretherton and Wyant, 1997), but they are also strongly influenced by the large-scale subsidence and the strength of the inversion capping the stratocumulus-topped boundary layer (Sandu *et al.*, 2010; Sandu and Stevens, 2011). SCTs over warm surface waters with weak capping inversions are generally faster (transition within approximately one day) than SCTs over cold waters with strong capping inversions (transition within four days) as these factors influence the turbulent mixing within the marine boundary layer. Other variables such as precipitation intensity and the amount of downwelling longwave radiation also affect the rate of the cloud cover change associated with SCT (Sandu and Stevens, 2011).

An SCT feedback as a result of global warming, with decreased Sc cloud cover and an increased amount of shallow cumulus clouds, has been suggested based on observations (Eastman *et al.*, 2011) and large eddy simulation (LES, Schneider *et al.*, 2019). However, the amount of change of different cloud types is highly uncertain and provides the largest source of disagreement in subtropical cloud feedbacks in general circulation models (GCMs) (Bony and Dufresne, 2005; Soden and Vecchi, 2011; Ceppi *et al.*, 2017). Observations also show a large spread in tropical low cloud cover change with temperature. Depending on the region of study, the data source, and the type of cloud considered, the feedback may be either positive or negative (Clement *et al.*, 2009; Bellomo *et al.*, 2014; McCoy *et al.*, 2017). Experiments using LES demonstrate that the difference in response may be explained by several counteracting processes (Blossey *et al.*, 2013; Bretherton, 2015). These processes are of more or less importance in different regions and may be resolved or parameterized in different ways in GCMs (Brient and Bony, 2013; Zhang *et al.*, 2013; Vial *et al.*, 2016). For example, Yamaguchi *et al.* (2017) showed that prognostic cloud droplet number concentrations (CDNCs), as well as cloud- and precipitation-related sinks of aerosol or CDNC, can promote a more rapid SCT than fixed CDNCs in LES, as the former gives rise to more drizzle and thus an accelerated reduction in Sc cloud cover.

Representing marine Sc microphysics and dynamics in GCMs is in general a challenging task. The amount and properties of the clouds rely on a range of parameterized processes and their interactions also influence the transition of Sc to trade cumulus. Progress has been made over the years in understanding marine Sc and SCT, especially in the LES community, but large-scale models still typically suffer from a "too few too bright" cloud problem (Karlsson *et al.*, 2008; Nam *et al.*, 2012; Konsta *et al.*, 2022). SCTs were, for example, the focus of an early GCSS (GEWEX Cloud System Study) model intercomparison study (Bretherton *et al.* 1999; Svensson *et al.*, 2000), which recently was repeated for state-of-the-art boundary-layer parameterizations, showing that many of the problems identified earlier persist (Neggers *et al.*, 2017). The rapid increase in computing power makes it possible to increase the horizontal resolution of GCMs, which could improve the representation of some of the processes important for low-level Sc clouds and their feedbacks. Other options would be to increase the vertical resolution to improve the representation of thermodynamics gradients, such as the temperature inversion capping the boundary layer, include more explicit descriptions of different cloud microphysical processes in GCMs, or to increase the level of complexity of the parameterizations.

In the atmosphere, aerosol particles act as cloud condensation nuclei and are crucial for cloud formation. A change in the number, size or composition of aerosols may affect the CDNC, drizzle production and other microphysical variables important for Sc formation, properties and SCT. However, aiming at accurately representing atmospheric aerosols and their effect on clouds in models is computationally very expensive – and also notoriously difficult. Still, the level of complexity of these parameterizations is known to enhance the performance of models in terms of reproducing observed temperature trends or physical phenomena (Wilcox *et al.*, 2013; Ekman, 2014; Kodros and Pierce, 2017; Yamaguchi *et al.*, 2017). To save computational power, especially when using high horizontal resolution, GCMs often make use of prescribed aerosol or cloud condensation nuclei fields. It is currently not clear how this type of simplified representation affects low-level tropical clouds or their feedback on climate change. Bulatovic *et al.* (2019) used LES to show that the shortwave cloud radiative effect of a marine stratocumulus cloud can be three times as large in simulations with fixed CDNCs compared to prognostic CDNC.

In the present study, we examine how the simulated radiative and microphysical properties of marine stratocumulus and SCTs are affected by different horizontal resolution (~135, 60 and 25 km, respectively) and different levels of complexity of the aerosol–cloud interaction parameterization in the Hadley Centre Global Environmental Model (HadGEM3) Global Coupled version 3.1 (HadGEM3-GC3.1; Williams *et al.*, 2017). The latter is done by comparing a model version that uses prescribed monthly average values of aerosol optical properties and CDNC with a model version where the number and mass concentrations of different types of aerosols are predicted at each model time step and where the aerosols are explicitly interacting with clouds and precipitation processes. We focus the analysis on the Sc regions defined in Klein and Hartmann (1993) and transects inspired by the GCSS/WGNE Pacific Cross-Section Intercomparison (GPCI) project (Teixeira *et al.*, 2011). Section 2 describes the HadGEM3-GC3.1 model, the different model versions used, and the simulation output used for the analysis. The selected marine stratocumulus regions and transects are also described. The results are presented in Section 3 and discussed in Section 4. Conclusions are drawn in Section 5.

2 | METHOD

2.1 | The Hadley Centre Global Environmental Model Global Coupled version 3.1

We use model output from the atmosphere-only version of the HadGEM3-GC3.1 (Williams *et al.*, 2017; Kuhlbrodt *et al.*, 2018; Menary *et al.*, 2018), which we hereafter refer to as HadGEM3. HadGEM3 uses the Prognostic Cloud fraction Prognostic Condensate (PC2) cloud scheme (Wilson *et al.*, 2008), and the Suite Of Community RAdiative Transfer (SOCRATES) radiative transfer code (a rewritten version of Edwards and Slingo, 1996). In PC2, mass mixing ratios of cloud liquid condensate and cloud ice condensate are prognostic variables along with liquid cloud volume fraction and ice cloud volume fraction. CDNCs are either prescribed (non-interactive version using the EasyAerosol module) or calculated interactively (interactive version using the GLOMAP aerosol module) and the CDNCs affect the autoconversion rates. The large-scale warm rain precipitation scheme is based on Boutle *et al.* (2014a), which includes a prognostic rain formulation and three-dimensional advection of the precipitation mass mixing ratios. The autoconversion rate is parameterized according to Khairoutdinov and Kogan (2000), with a bias correction introduced by Boutle *et al.* (2014b) to represent the effect of sub-grid variability on autoconversion and accretion rates. Fall velocities and rain-rate-dependent particle size distributions follow Abel and Boutle (2012) and Abel and Shipway (2007), respectively. Note that the number concentrations of raindrops and ice hydrometeors are not explicitly predicted by the model. In SOCRATES, the raindrop size distribution is calculated from the CDNC following Liu *et al.* (2008), where the widening of the cloud droplet spectrum with increasing cloud condensation nuclei is accounted for. To achieve an adequate representation of in-column evaporation, the precipitation scheme is also called with a higher frequency (every 2 min) than the atmospheric model time step of 20 min. For boundary-layer mixing, the model uses the first-order turbulence closure scheme of Lock *et al.* (2000) with the modifications described in Lock (2001) and Brown *et al.* (2008). Further details on the atmospheric part of the model and the different parameterization schemes are found in Walters *et al.* (2019).

GLOMAP (Global Model of Aerosol Processes) is a part of the United Kingdom Chemistry and Aerosol (UKCA) model. The version of GLOMAP used here, GLOMAP-mode (Mann *et al.*, 2010; Bellouin *et al.*, 2013), simulates aerosol mass and number concentrations in five size modes, using a "pseudo-modal" aerosol dynamics approach. This approach implies that the size distribution of aerosols within each mode is assumed to be log-normal, but the size distribution is simplified to a single diameter in each mode when calculating aerosol process rates (i.e., primary emissions, dry deposition, sedimentation, scavenging, aging, hygroscopic growth, nucleation of new particles, coagulation, condensation and cloud processing). The chemistry part of UKCA determines oxidation and aging rates that affect the formation and evolution of aerosols in GLOMAP. Four different aerosol components are considered: sulfate, black carbon, organic matter and sea salt. These components are internally mixed within each mode. The composition of each mode affects the refractive index of the mixture, which is calculated interactively by volume averaging. Mineral dust is calculated separately from the other aerosol types using the CLASSIC scheme (Bellouin *et al.* 2011) and is not part of the GLOMAP framework. It can therefore be considered as externally mixed with the other GLOMAP aerosol components. Look-up tables based on Mie theory are used to obtain aerosol optical properties which in turn affect the modeled radiation.

A Köhler-theory-based aerosol activation parameterization (Abdul-Razzak and Ghan, 2000; West *et al.*, 2014) is used to diagnose CDNC based on the GLOMAP aerosol size distribution and composition. The diagnostic CDNC is then used in the calculation of liquid cloud droplet effective radius (Martin *et al.*, 1994) and in the calculation of autoconversion of cloud droplets to precipitation

(West *et al.*, 2014), that is, to simulate aerosol indirect effects. In HadGEM3, autoconversion only occurs when the number concentration of cloud droplets with radius larger than 20 μm exceeds 1,000 m^{-3}, found by assuming a Khrgian–Mazin-modified gamma cloud droplet size distribution. Nucleation and impaction scavenging of aerosols follows the approach by Mann *et al.* (2010), where the removal rates are proportional to the modeled precipitation rates. There are no interactions between aerosols and ice clouds in HadGEM3. Historical emissions of aerosols and aerosol emissions follow Hoesly *et al.* (2018).

The EasyAerosol module within HadGEM3 prescribes monthly averages of aerosol optical properties (aerosol extinction, absorption, and asymmetry parameter averaged over the six shortwave and nine longwave wavebands of SOCRATES) as well as prescribed CDNCs to calculate the effect of aerosols on radiation, liquid cloud albedo and liquid precipitation formation. Background values of the optical variables and CDNCs are obtained from a HadGEM3 simulation using GLOMAP and aerosol emissions corresponding to pre-industrial conditions (year 1850). The MACv2-SP framework (Stevens *et al.*, 2017) is then used to perturb the background variables, that is, to add anthropogenic perturbations to aerosol optical properties and CDNC on top of the background values.

2.2 | Experimental design

Our analysis is based on output for the years 1978–2008 from four simulations which were forced with prescribed sea surface temperatures (SSTs) (Table 1). High-resolution daily SSTs and sea ice concentrations from the Hadley Centre Sea Ice and Sea Surface Temperature data set version 2.2 on a 0.25° grid (HadISST2.2; Kennedy *et al.*, 2017) were used in all simulations and remapped to the respective model grid. The simulations using EasyAerosol span over three horizontal resolutions: high (N512, ~25 km), medium (N216, ~60 km) and low (N96, ~135 km), respectively, using the same vertical resolution of 85 pressure levels in the atmosphere, where 10 levels are below approximately 800 m (Roberts *et al.*, 2019). All simulations use the same tuning configuration (Roberts *et al.*, 2019). The medium resolution simulation was also repeated with the interactive high-complexity aerosol scheme GLOMAP. The only difference between the two simulations with medium resolution (shown in Table 1) is the way aerosols and their climate effects are represented: either fully interactive aerosol–cloud and aerosol–radiation interactions using GLOMAP or prescribed aerosol optical properties and CDNC from GLOMAP + MACv2-SP using the EasyAerosol approach. All four model configurations were used for the sixth Climate Model Intercomparison Project (CMIP6); the EasyAerosol versions were used for the HighResMIP simulations while the GLOMAP version was used for a selection of other MIPs.

TABLE 1 List of simulations used in the analysis. N is the number of latitude points between the pole and equator on a Gaussian grid

Simulation name	Resolution	Aerosol representation
HiRes-EA	N512	Non-interactive aerosols (EasyAerosol)
MedRes-EA	N216	Non-interactive aerosols (EasyAerosol)
MedRes-GLOMAP	N216	Interactive aerosols (GLOMAP)
LowRes-EA	N96	Non-interactive aerosols (EasyAerosol)

All analyzed variables presented in Sections 3.1 and 3.2 are presented for the spring season in each hemisphere (March–April–May in the northern hemisphere and September–October–November in the southern hemisphere) as this is the season with maximum low-level cloud cover (cf. Hahn and Warren, 2007; Wood, 2012, and Figure A1). Seasonal averages of monthly model output are analyzed, except for precipitation where seasonal averages of three-hourly output are also calculated. Output for aerosol optical depth (AOD) and CDNC was only available for MedRes-GLOMAP and LowRes-EA. However, the AOD and CDNC fields applied in MedRes-EA and HighRes-EA are equivalent to the ones in LowRes-EA, as they were interpolated from the low-resolution grid to the higher resolutions. Note that all CDNCs are weighted by cloud fraction, effectively giving cloud-free sky a weight of zero. The statistical significance of any presented difference has been calculated using a two-sided Student's *t*-test at the 95% level. In the following, "significant" refers to statistically significant results.

2.3 | Definition of marine stratocumulus regions and transects

Four regions (cf. Figure 1) with persistent marine Sc cloud cover along the western coasts of South America (Peruvian region), Southern Africa (Namibian region), North America (Californian region) and Northern Africa (Canarian) taken from Klein and Hartmann (1993) are analyzed. Due to the difference in model resolution (Table 1), the size of each area differs slightly between the simulations. Similarly, four transects consisting of eight to 10 grid points originating in the Sc regions are selected: Northeast Atlantic (NEA), Northeast Pacific (NEP), Southeast

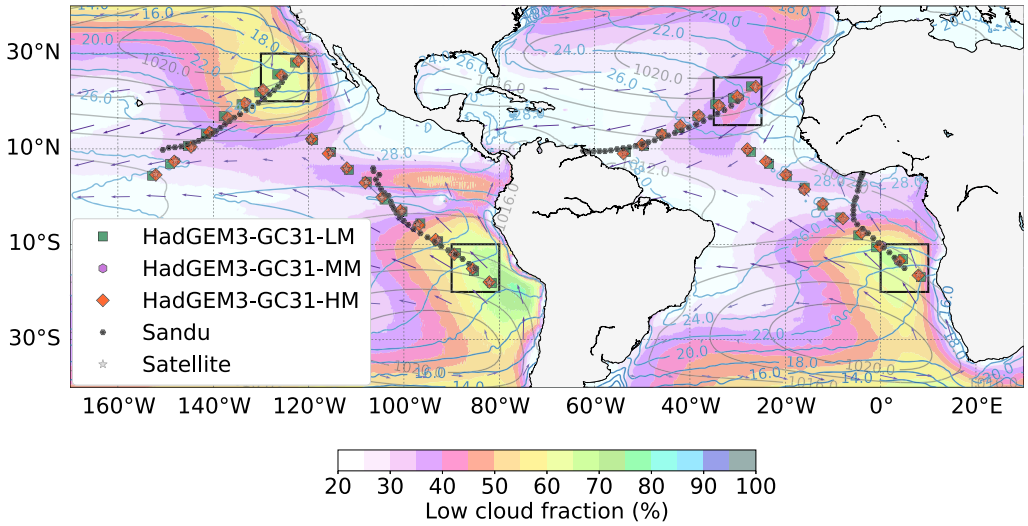

FIGURE 1 Grid point positions along the North East Atlantic (NEA), North East Pacific (NEP), South East Pacific (SEP) and South East Atlantic (SEA) transects for different horizontal resolution versions of HadGEM3. Black dots mark the mean air mass trajectories from Sandu *et al.* (2010). Background map shows the climatology of sea surface temperature (unfilled contours), mean sea level pressure (gray), winds (arrows) and low cloud cover for 1978–2008 from ERA5 reanalysis. The gray boxes display the four stratocumulus regions: Canarian, Californian, Peruvian and Namibian [Colour figure can be viewed at wileyonlinelibrary.com]

Atlantic (SEA) and Southeast Pacific (SEP) transects (Figure 1). The grid positions of the transects were determined based on Sandu *et al.* (2010) who used reanalysis data to calculate boundary-layer air mass trajectories. Due to the different horizontal resolutions of the different model versions, the grid point positions, in latitudinal steps of around 2° and longitudinal steps of around 4°, along the transects do not completely intersect and the closest grid points along the predefined transect were sampled from each simulation, see Figure 1. Also shown is the yearly climatology of SSTs for 1978–2008 along with surface winds and low cloud cover based on ERA5 reanalysis (Hersbach *et al.*, 2020). The transects generally follow the trade winds over the SST gradients toward the equator. They are situated in the subtropical–tropical part of the Hadley circulation (see Figure 2, please note the logarithmic height axis), beginning in the subsidence region. Toward the equator, all transects except NEA display positive vertical motion, that is, a "region of deep convection." In between the Sc and region of deep convection, there is a "transition region." Only very small and non-significant differences between the simulations are found in the near-surface mean wind speed and the statistically-preferred wind direction along the transects (not shown).

2.4 | Satellite retrievals

We use satellite-retrieved values of AOD at 550 nm, cloud liquid water path, precipitation, and radiation fluxes in our evaluation of the model results. AOD values are obtained from the obs4MIPs archive (https://esgf-node.llnl.gov), and are based on the Moderate Resolution Imaging Spectroradiometer (MODIS) level 2 product (Levy *et al.*, 2009) for the years 2000–2012. Cloud liquid water path is calculated as an average over the years 1988–2016 using aggregated observations from multiple satellite microwave sensors (MAC-LWP, Elsaesser *et al.*, 2017). The LWP retrievals are associated with uncertainty, but are in general most reliable in regions with a low ratio between precipitation and liquid water path, which is also the case for the Sc regions (Elsaesser *et al.*, 2017). Precipitation data are obtained from the Global Precipitation Climatology Project (GPCP) Climate Data Record Version 2.3 (Adler *et al.*, 2016; 2018) for the years 1979–2008 while for radiation fluxes, data from the Clouds and the Earth's Radiant Energy System (CERES) Energy Balanced and Filled (EBAF, Loeb *et al.*, 2018) Ed. 4.1 for the years 2000–2021 was used. Note that we have chosen to use the longest time period available for all satellite data, and that they all span different time periods than the simulations (1978–2008).

3 | RESULTS

3.1 | Microphysical and radiative properties of marine stratocumulus

CDNC values are typically higher with interactive than with non-interactive aerosols, at least within the main low-level cloud layer, and differences are larger

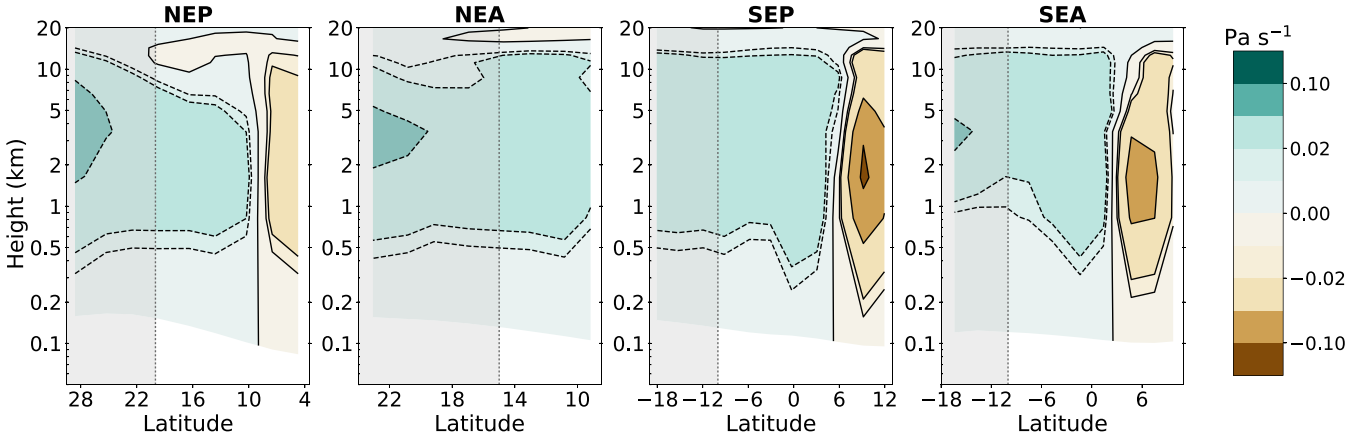

FIGURE 2 Mean vertical cross-section of subsidence (Pa s^{-1}) from the MedRes-EA simulation for all transects (from left to right: NEP, NEA, SEP, SEA) for the spring season in each hemisphere. The stratocumulus regions are marked with shaded boxes [Colour figure can be viewed at wileyonlinelibrary.com]

over the northern-than southern-hemisphere regions (Figure 3). Close to the surface, that is, below approximately 200 m altitude, the CDNC tends to be higher with non-interactive than with interactive aerosols. The generally higher CDNCs with interactive aerosols are consistent with the AOD values, which are 16%–28% higher in MedRes-GLOMAP than in MedRes-EA (Table 2), and suggest that the aerosol concentrations are also higher with interactive compared to non-interactive aerosols. These differences highlight the impossibility of reproducing a time-averaged prescription of CDNC with instantaneous simulations where CDNC is derived from interactive aerosols numbers. Note that the AOD is obtained differently and independently in the GLOMAP and EasyAerosol modules so the distributions differ between the two model versions. Nevertheless, regardless of the aerosol module, AOD is clearly underestimated over all regions compared to the MODIS retrievals but is somewhat closer to the retrievals with interactive compared to non-interactive aerosols, as shown in Table 2. The difference is larger over the regions in the northern hemisphere (Californian and Canarian) than in the southern hemisphere (Namibian and Peruvian).

For the northern-hemisphere Sc regions (Californian and Canarian), neither the horizontal resolution nor the aerosol–cloud interaction parameterization complexity has a large impact on the liquid water path of the stratocumulus clouds; the differences are generally less than 5% (Figure 4 and Table 2). However, the simulation with low resolution (LowRes-EA) has less liquid water than all other simulations and the differences are significant in the Canarian region. For the southern-hemisphere Namibian and Peruvian regions, the differences between the different model versions are more pronounced than over the southern-hemisphere regions. The liquid water amount increases significantly with increasing model resolution and the simulation with non-interactive aerosols (MedRes-EA) has significantly more liquid water than the simulation with interactive aerosols (MedRes-GLOMAP). This liquid water increase happens despite smaller CDNCs in MedRes-EA, suggesting that either changes in cloud processes (as a response to changes in autoconversion) or confounding responses due to cloud dynamics or internal variability affect the overall liquid water response. A closer examination of the mean subsidence rates in the subtropics in MedRes-EA and MedRes-GLOMAP (not shown) also shows that the subsidence rates are somewhat higher in the subtropics in MedRes-EA. All model versions overestimate the liquid water path compared to the MAC-LWP dataset. The simulation with low resolution (LowRes-EA) is closest to the retrievals and is within one standard deviation over the Californian region.

Differences in seasonal mean precipitation rates calculated based on monthly average output are generally very small and non-significant (not shown). However, if three-hourly output data are used (which was only available for precipitation rates), then interactive aerosols (MedRes-GLOMAP) give significantly higher precipitation rates than non-interactive aerosols (MedRes-EA), except over the Canarian region (Table 2). The differences in domain-averaged precipitation rates are very low, only a fraction of a mm per day, but these types of small differences may still be important for the dynamics of the stratocumulus clouds (Svensson *et al.*, 2000). Changing the model resolution gives no clear change in domain-averaged three-hourly precipitation rates. All model versions clearly underestimate the precipitation rates compared to satellite retrievals over the Californian and Canarian regions. Over the Namibian and Peruvian

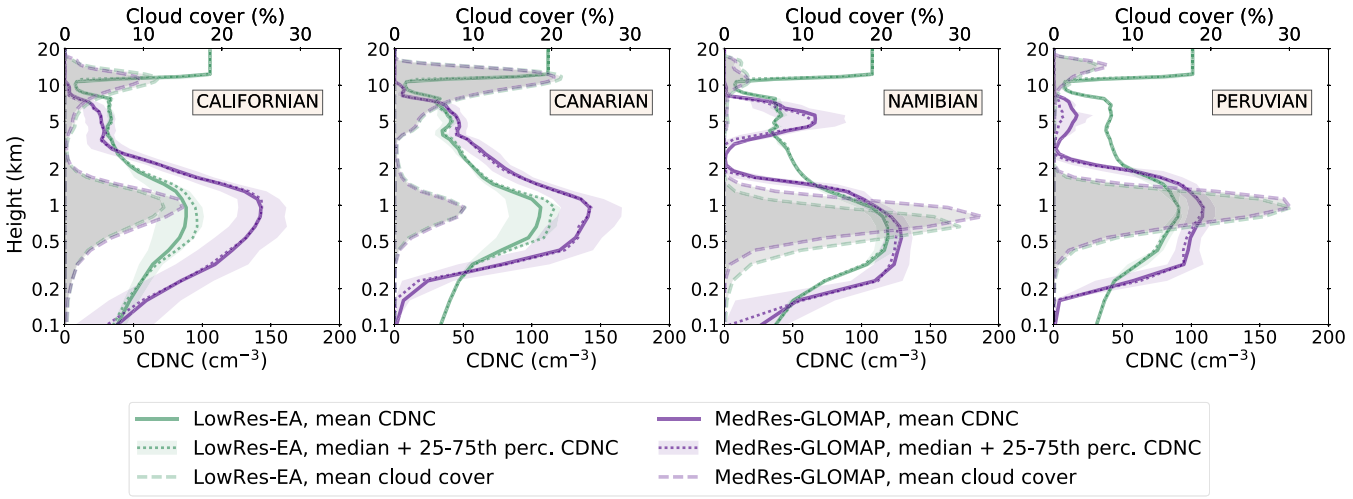

FIGURE 3 Mean (solid line) and median (dotted lines) vertical distribution of cloud droplet number concentration (CDNC) [cm^{-3}] for MedRes-GLOMAP and LowRes-EA for the spring season in each hemisphere and for all regions (from left to right: Californian, Canarian, Namibian, Peruvian, cf. also Figure 4). Color shadings indicate 25th to 75th percentiles of CDNC. Gray-shaded regions bounded by dashed lines indicate mean cloud cover (%) in the two simulations (includes both liquid and ice). Note that the CDNC fields in LowRes-EA and MedRes-EA are equivalent (see Section 2.2) [Colour figure can be viewed at wileyonlinelibrary.com]

regions, all model versions are close to observations (underestimate less than 20%).

The shortwave (SW) cloud radiative effect (CRE) at the top of the atmosphere (TOA) becomes stronger (more negative) with increasing resolution and the differences are more pronounced over the southern-hemisphere regions (up to 10 W m^{-2} comparing low and medium resolution), in agreement with the differences in liquid water path. The results are more complex when comparing the simulations with different aerosol complexity. For the Californian and Canarian regions, the SW CRE is stronger (about 1–2 W m^{-2}) when using interactive (MedRes-GLOMAP) compared to non-interactive (MedRes-EA) aerosols, most likely as a result of the slightly higher CDNC (Figure 3) and the relatively similar liquid water paths (Table 2). Over the Namibian and Peruvian regions, the SW CRE is weaker (between 2 and 6 W m^{-2}) in MedRes-GLOMAP compared to MedRes-EA as a result of the lower liquid water path with interactive aerosols (Table 2) and similar CDNC values (Figure 3). All model versions are in reasonable agreement with the satellite data considering the large standard deviation in the observations (Table 2). However, HiRes-EA overestimates the SW CRE over the Canarian and Peruvian regions. In general, the use of interactive instead of non-interactive aerosols brings the model closer to the observed mean of the SW CRE. The differences between the different model versions in the simulated net SW radiation at the TOA largely reflect the changes in the SW CRE (Table 2). However, the differences in the net SW radiation at TOA are generally non-significant, most likely due to the larger spatial and temporal variability. All model versions underestimate the net all-sky radiation at TOA compared to the satellite retrievals.

3.2 | Marine stratocumulus-to-cumulus transition

The CDNC within the low-level cloud layer is either higher or similar with interactive aerosols compared to with non-interactive aerosols (Figure 5). The exception is the SEA region where the CDNC is sometimes substantially lower in MedRes-GLOMAP compared to LowRes-EA, in particular within the region of deep convection. Figure 6 shows the vertical cross-section of cloud liquid water together with the mean cloud fraction for the spring season in each hemisphere. All HADGEM3 versions show the general features of a SCT over all regions except the NEA (cf. Figure 2): within the higher latitudes of the subtropics there are shallow liquid stratocumulus clouds. These clouds tend to thicken with decreasing latitude as the height of the capping boundary-layer inversion increases. At lower latitudes within the sub-tropics, the cloud type shifts to broken cumulus and the average liquid water content decreases. Close to the equator, the main cloud type is deep convective clouds. Similar to the Sc regions analyzed in Section 3.1, the differences in cloud liquid water for the northern-hemisphere transects (NEP and NEA) are generally small and non-significant. This result is even more clear in Figure 7 which shows the cloud liquid water path along the transects. It is only the LowRes-EA that gives a discernable difference compared to the other model

TABLE 2 Mean values of different quantities for all simulations and all stratocumulus regions during their respective spring season (March–April–May for the northern hemisphere and September–October–November for the southern hemisphere)

	LowRes-EA	MedRes-EA	MedRes-GLOMAP	HiRes-EA	Satellite
Aerosol optical depth (@ 550 nm)					
Californian	*0.089*	*0.089*	**0.106**[a]	*0.089*	0.14 ± 0.02
Canarian	*0.172*	*0.172*	**0.207**[a]	*0.172*	0.22 ± 0.02
Namibian	*0.166*	*0.166*	**0.205**[a]	*0.166*	0.33 ± 0.02
Peruvian	*0.072*	*0.072*	**0.100**[a]	*0.072*	0.12 ± 0.01
Cloud liquid water path [g m^{-2}]					
Californian	52.6	*55.2*	57.1	55.1	48.1 ± 5.1
Canarian	**33.7**	*36.7*	36.3	38.3	26.3 ± 3.7
Namibian	**54.1**	*70.0*	**64.4**	**75.4**	47.6 ± 4.6
Peruvian	**84.4**	*95.8*	**91.3**	**99.3**	79.4 ± 4.7
Precipitation [mm day^{-1}]					
Californian	**0.39**	*0.36*	**0.41**	0.37	0.54 [0.12,1.78]
Canarian	**0.37**	*0.39*	0.38	**0.32**	0.60 [0.06,1.12]
Namibian	**0.12**	*0.13*	**0.14**	0.13	0.15 [0.03,0.21]
Peruvian	**0.14**	*0.13*	**0.14**	**0.15**	0.16 [0.01,0.20]
Shortwave cloud radiative effect at top of the atmosphere [W m^{-2}]					
Californian	**−59.2**	*−63.2*	**−66.6**	−64.0	−66.8 ± 13.2
Canarian	**−35.0**	*−38.5*	−39.7	−40.4	−30.5 ± 9.4
Namibian	**−61.8**	*−72.1*	**−66.2**	**−74.3**	−63.4 ± 11.8
Peruvian	**−77.1**	*−82.5*	**−80.2**	**−84.9**	−71.2 ± 11.2
Net all-sky shortwave radiation at top of the atmosphere [W m^{-2}]					
Californian	325.6	*321.7*	318.0	320.1	272.3 ± 13.7
Canarian	351.3	*348.1*	347.2	346.2	316.8 ± 9.7
Namibian	**331.4**	*321.2*	326.9	319.0	295.6 ± 12.1
Peruvian	318.3	*312.9*	314.9	310.6	290.1 ± 11.6

Note: All values are based on monthly mean output except precipitation, which is based on three-hourly output. Significant differences compared to the reference (MedRes-EA, marked in italic) are marked with bold font. Cloud liquid water path values are for all-sky. Satellite-retrieved mean values and standard deviations are shown in the rightmost column and are described further in Section 2.4. For precipitation, the 10- and 90-percentile range is given instead of the standard deviation.

[a] AOD is only compared between MedRes-GLOMAP and LowRes-EA because AOD in MedRes-EA and HiRes-EA is simply an interpolation of LowRes-EA AOD.

versions (as indicated by the significance level), and only in the deep convection part of the NEP and NEA transects. Deep convection parameterizations and corresponding cloud fields are known to be sensitive to horizontal resolution (e.g., Phillips *et al.*, 1995), an issue that is not the focus of the present study and that will not be investigated further. For the southern-hemisphere transects (SEP and SEA), the differences in cloud features are also small (due to either a change in resolution or aerosol complexity) and not easily distinguished when displayed as vertical cross-sections (Figure 6). However, Figure 7 shows that there are indeed substantial differences in integrated liquid water over both the stratocumulus regions and the transition regions, in particular for SEA. The liquid water content is in general higher with higher resolution and with non-interactive aerosols.

The mean precipitation rates along the transects are similar in all model versions when comparing seasonal averages based on monthly average model output (not shown). However, with three-hourly output for precipitation rates (Figure 8), all regions show statistically significant differences between the HadGEM3-GLOMAP and HadGEM3-EasyAerosol simulations. Similar to Section 3.1, the differences in precipitation rates are only

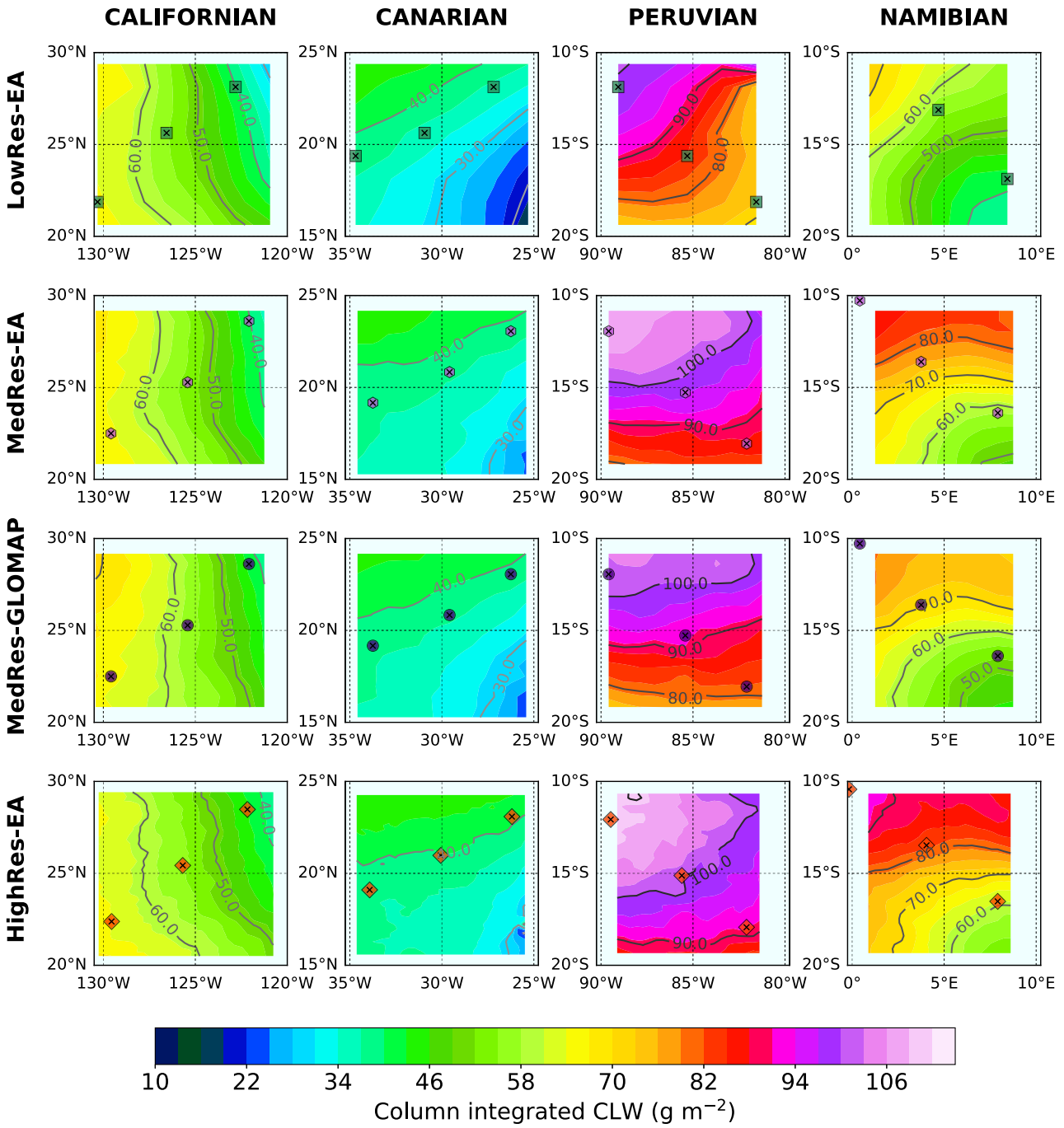

FIGURE 4 Horizontal distribution of column integrated all-sky liquid cloud water [CLW; g m^{-2}] for all versions of HadGEM3, for the spring season in each hemisphere and for all regions. Markers indicate transect positions (cf. Figure 1) [Colour figure can be viewed at wileyonlinelibrary.com]

a fraction of a mm per day, but this may still impact the SCT (Svensson *et al.*, 2000). Higher resolution and lower aerosol–cloud complexity generally result in lower precipitation rates, which is consistent with the higher liquid water paths (Figure 7). For all regions except NEP, this difference in precipitation rates is visible along most parts of the transects.

The SW CRE at TOA is in general slightly larger (i.e., more negative) over all Sc and transition regions when increasing the horizontal resolution from low to medium (Figure 9). For the southern-hemisphere regions, this result is in agreement with the higher liquid water paths (Figure 7). Over the northern-hemisphere regions, the reason for the difference is more unclear, but could be related to somewhat higher cloud fractions in MedRes-EA compared to LowRes-EA (Figure 6). The difference between the simulations with interactive and non-interactive aerosols is more complex. For

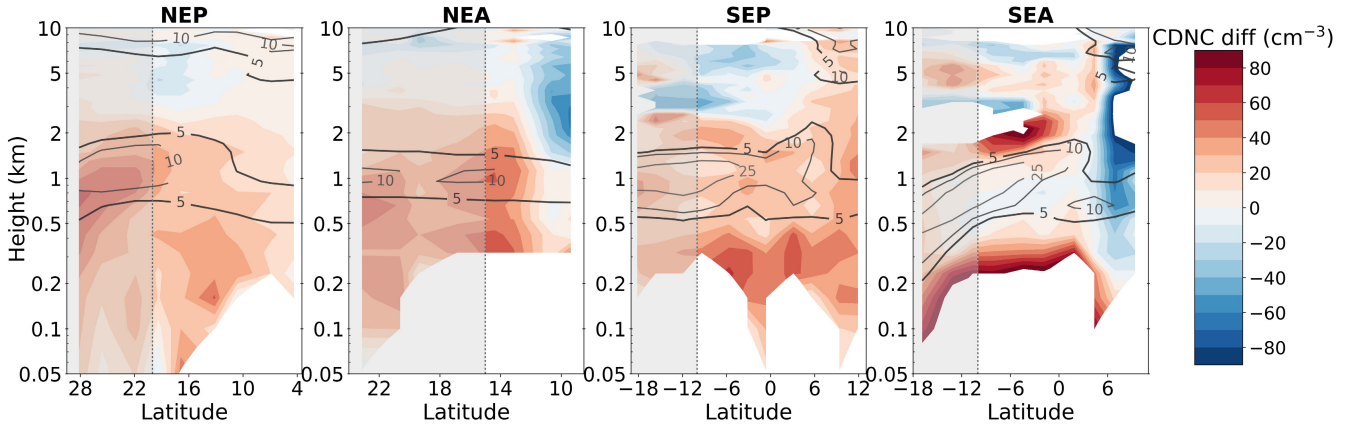

FIGURE 5 Mean difference in cloud droplet number concentration [cm^{-3}] between MedRes-GLOMAP and LowRes-EA for the spring season in each hemisphere and for all transects (from left to right: NEP, NEA, SEP, SEA, cf. Figure 1). Stratocumulus regions are marked with gray-shaded boxes. Gray isolines indicate 5%, 10%, 25%, and 50% cloud fraction (both liquid and ice, from LowRes-EA) while colored isolines denote cloud droplet number concentration (CDNC) differences equal to −60, −30, 0, 30 and 60 cm^{-3}. Note that the CDNC fields in LowRes-EA and MedRes-EA are equivalent (see Section 2.2) [Colour figure can be viewed at wileyonlinelibrary.com]

SEP and SEA, MedRes-GLOMAP shows a significantly smaller (less negative) CRE over both the Sc and the transition region. In these regions, the integrated cloud water was significantly lower in MedRes-GLOMAP compared to MedRes-EA while the CDNC values in MedRes-GLOMAP were similar or even slightly lower in MedRes-GLOMAP than in LowRes-EA (Figure 2b). For NEP, MedRes-GLOMAP shows a significantly larger (more negative) CRE over the Sc region than MedRes-EA, despite having about the same liquid water path values (Figure 7). The reason is most likely the substantially higher CDNCs in MedRes-GLOMAP compared to MedRes-EA (Figure 2b) resulting in a higher cloud albedo and a stronger CRE. Over the NEA, the differences in net CRE are small and non-significant despite relatively large differences in CDNC. Despite sometimes substantial differences in SW CRE between the different simulations, the impact on the all-sky SW radiation at TOA is in general small (less than ∼10 W m^{-2}) and not statistically significant (not shown).

4 | DISCUSSION

If the timing of the SCT is affected by the model representation of aerosol–cloud interactions or by the horizontal resolution, then there should be a visible change in the extent or location of the different transect regimes, that is, the extent of the Sc, transition and convective regions should be different. There is no such clear shift or change in the regimes in any of the transects (Figure 7). One possible exception is the low-resolution simulation (LowRes-EA) which for all regions shows a peak in the integrated liquid water content for the Sc regime at a slightly higher latitude compared to the other model versions, but the difference is less than 1°.

For the cloud microphysical and radiative properties, the analysis of the Sc and SCT regions in Sections 3.1 and 3.2 show consistent results. With increasing horizontal resolution, the liquid water content generally increases, which results in a more negative SW CRE. The effect is stronger over the southern than northern-hemisphere SCT transects and Sc regions, most likely due to the overall higher cloud fraction over the southern-hemisphere Sc regions (Figure 1).A higher horizontal resolution should result in better resolved horizontal temperature gradients, which may affect inversion strength, winds and thereby turbulence and subsequently the source of moisture to the stratocumulus cloud. Thomas *et al.* (2019) examined the global impact of model resolution on SW CRE in four different models and obtained qualitatively similar results as ours for the marine Sc regions (see figures 2 and 3 in their study). Furthermore, Terai *et al.* (2020) compared a global model that resolves sub-kilometer scales with a coarser-resolution version of the same model and found that the former produced higher liquid water paths than the latter.

The influence of a change in the aerosol–cloud interaction complexity is less straight-forward to analyze. Not only is the absolute aerosol amount different for the different model versions (cf. Table 2 and Figure 5), but the aerosol population in GLOMAP will also vary at each model time step while the EasyAerosol versions of HadGEM3 use fixed monthly values of CDNC and AODs. Non-linearities in aerosol–cloud interactions may therefore give rise to somewhat counterintuitive results. For example, the prescribed CDNCs applied in the EasyAerosol versions of HadGEM3 are typically

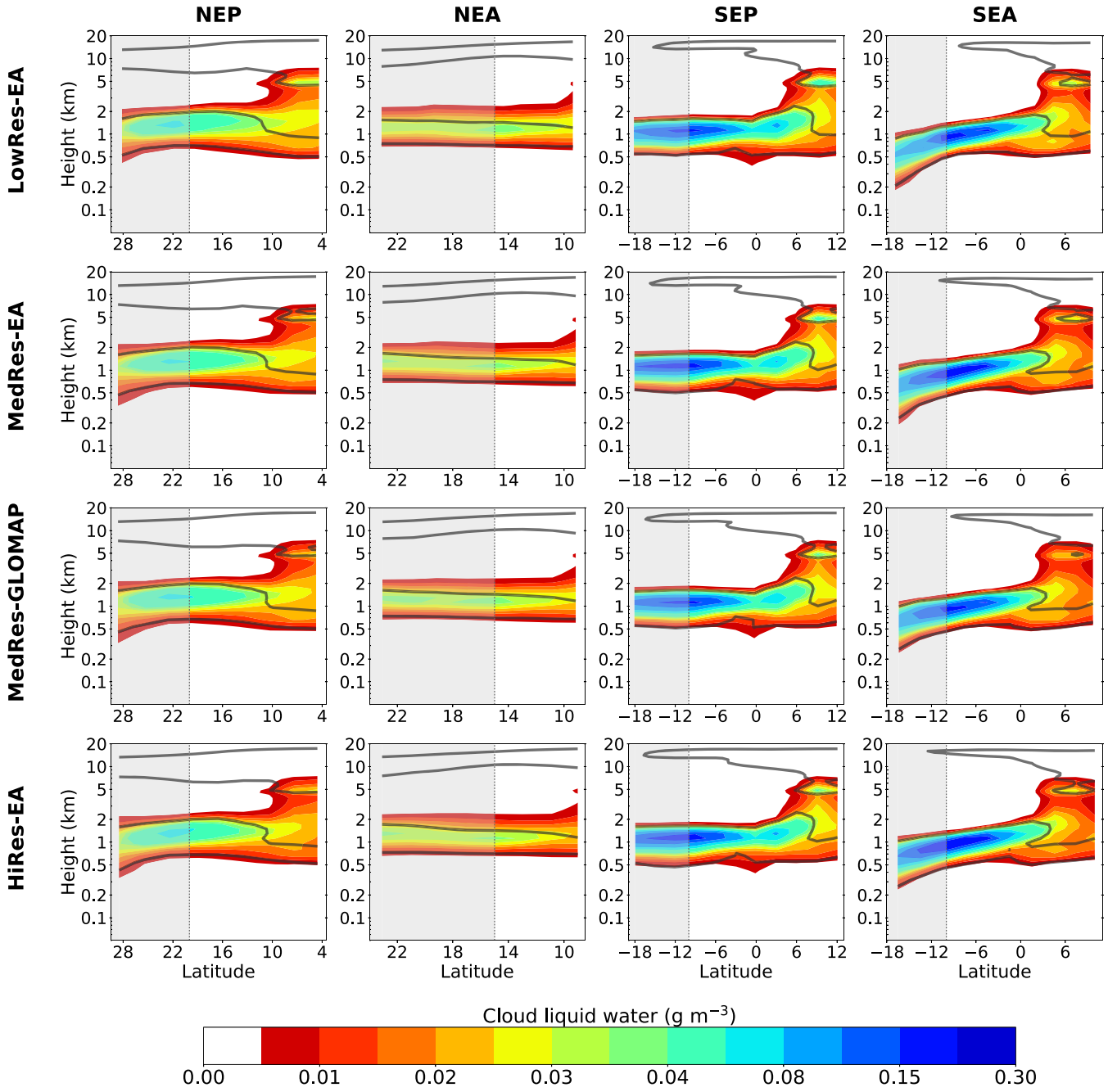

FIGURE 6 Mean vertical cross-section of cloud liquid water (colors) and the mean cloud fraction (contours) for all versions of HadGEM3 (from top to bottom: LowRes-EA, MedRes-EA, MedRes-GLOMAP, MedRes-EA) for all transects (left to right: NEP, NEA, SEP, SEA) for the spring season in each hemisphere. Isolines denote 5% cloud fraction. Stratocumulus regions are marked with gray-shaded boxes [Colour figure can be viewed at wileyonlinelibrary.com]

lower than the values obtained using MedRes-GLOMAP (Figures 3 and 5). However, the precipitation rates are also lower (Figure 8 and Table 2). The latter result leads to higher liquid water content in MedRes-EA than in MedRes-GLOMAP, in particular over the southern-hemisphere transects and Sc regions. For the southern hemisphere, the difference in SW CRE is dominated by the change in liquid water content and the SW CRE is larger (more negative) with non-interactive aerosols (MedRes-EA) than with interactive aerosols (MedRes-GLOMAP). In the northern hemisphere, the change in CDNC plays a relatively larger role and the difference in SW CRE is either non-significant or even larger (more negative) in MedRes-GLOMAP than in MedRes-EA. In general, interactive aerosols bring the model closer to satellite-retrieved values of the SW CRE. The exception is over the Canarian region where the impact of interactive versus non-interactive aerosols is non-significant.

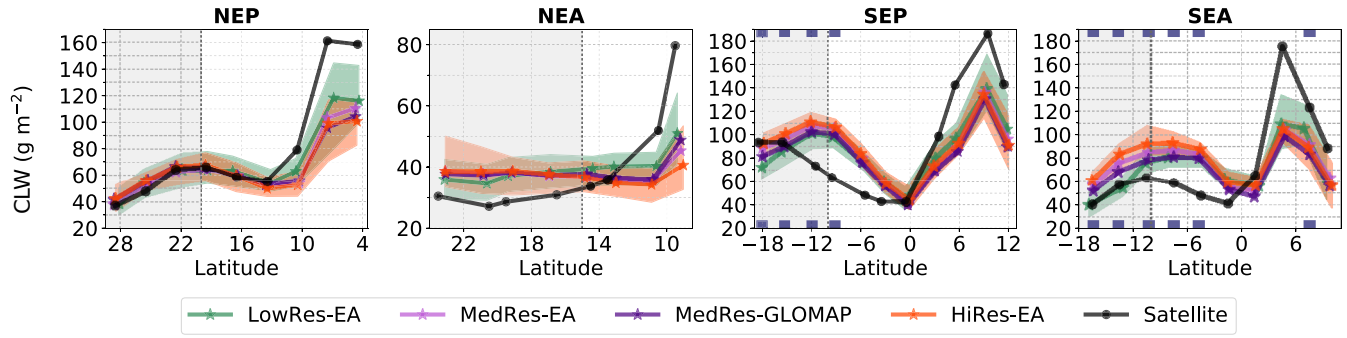

FIGURE 7 Mean integrated liquid cloud water path [CLW; g m^{-2}] for all versions of HadGEM3 (colors) and satellite retrievals (black) for all transects (left to right: NEP, NEA, SEP, SEA) for the spring season in each hemisphere. Statistically significant differences between MedRes-GLOMAP and MedRes-EA are marked with purple dots at the bottom and top of the figures. Shaded areas indicate 25th to 75th percentiles of the LowRes (green) and HighRes (orange) simulations. Stratocumulus regions are marked with gray-shaded boxes [Colour figure can be viewed at wileyonlinelibrary.com]

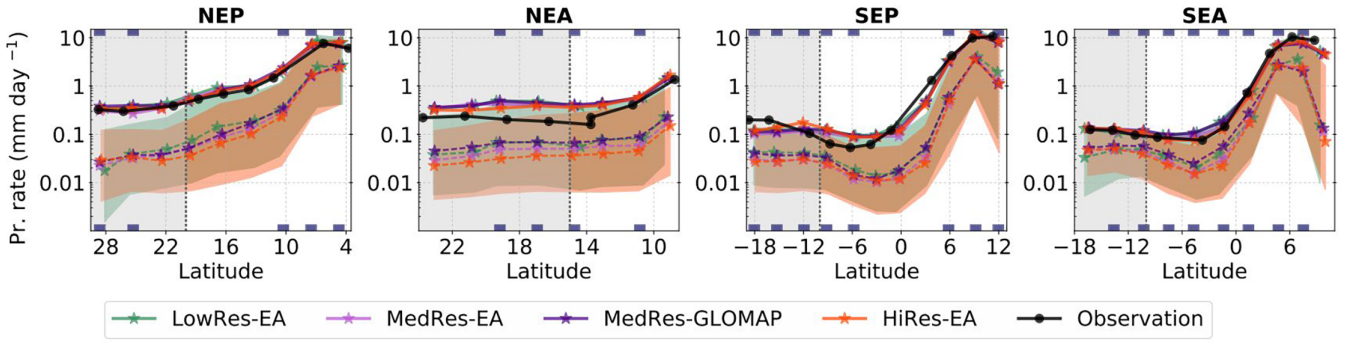

FIGURE 8 Mean (solid lines) and median (dashed lines) precipitation rates [mm day^{-1}] for all versions of HadGEM3 and (colors) and satellite retrievals (black) for all transects (left to right: NEP, NEA, SEP, SEA) for the spring season in each hemisphere using 3-hourly model output. Statistically significant differences between MedRes-GLOMAP and MedRes-EA are marked with purple dots at the bottom and top of the figures. Shaded areas indicate 25th to 75th percentiles of the LowRes (green) and HiRes simulations (orange). Stratocumulus regions are marked with gray-shaded boxes [Colour figure can be viewed at wileyonlinelibrary.com]

The impact of changes in model resolution and aerosol–cloud interaction complexity on modeled net TOA SW radiation was in Section 3.1 generally found to be non-significant, despite the significant changes in SW CRE. The reason is most likely the larger spatial and temporal variability in net TOA SW radiation compared to the SW CRE. However, a closer look at the clear-sky values of the net SW radiation at TOA (not shown) shows that the differences between the different model versions are generally small (less than 0.4 W m^{-2}) and non-significant, but nevertheless in the opposite direction to the differences found for the CRE. This result implies that changes in the SW clear-sky radiation may to some extent mask the changes in SW CRE induced by changes in the aerosol–cloud parameterization or by changes in model resolution. Nevertheless, the main reason for the non-significant changes in all-sky net TOA SW radiation is that the perturbations induced by changes in aerosol–cloud interaction parameterization or horizontal resolution are relatively small compared to the internal variability of the model.

In the sensitivity simulations, the vertical resolution was not changed although that has been shown to have an impact on Sc clouds (e.g., Xie *et al.*, 2018). Changing vertical resolution requires much more effort as parameterizations are not always independent of the vertical grid (Rasch *et al.*, 2019). In comparison with many other climate models, HadGEM3 has a fairly high vertical resolution but it is still very limited considering how thin Sc are and how dependent they are on interactions between turbulence, including entrainment, radiation and cloud microphysics. Another aspect that might influence the limited effects found here is that prescribed SSTs have been used; in coupled simulations, we expect to see larger changes, especially if the skin temperature has a diurnal cycle (e.g., Chen and Wang, 2016).

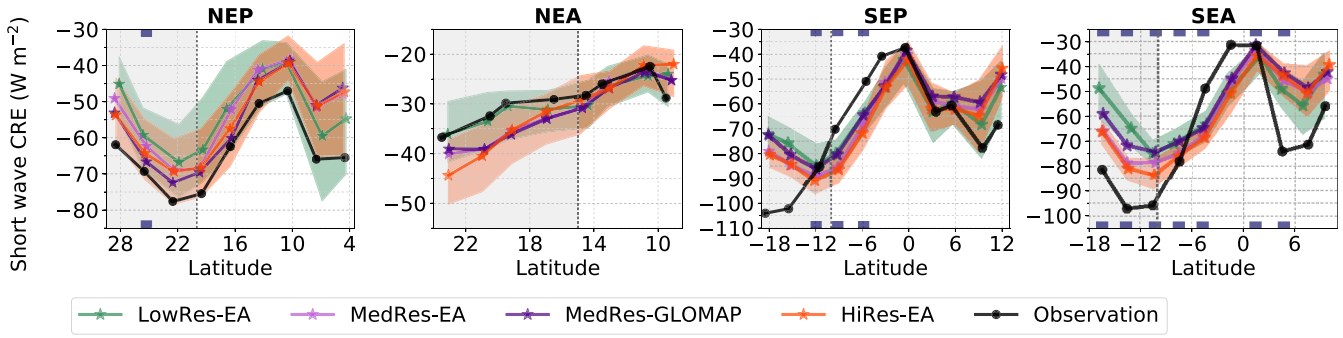

FIGURE 9 Mean short-wave cloud radiative effect [W m^{-2}] at the top of the atmosphere for all versions of HadGEM3 (colors) and satellite retrievals (black) for all transects (left to right: NEP, NEA, SEP, SEA) for the spring season in each hemisphere. Statistically significant differences between MedRes-GLOMAP and MedRes-EA are marked with purple dots at the bottom and top of the figures. Shaded areas indicate 25th to 75th percentiles of the LowRes (green) and HiRes simulations (orange). Please note the difference in vertical axes for the different regions. Stratocumulus regions are marked with gray-shaded boxes [Colour figure can be viewed at wileyonlinelibrary.com]

5 | SUMMARY AND CONCLUSIONS

In this study, we have used output from an atmosphere-only general circulation model (HadGEM3) to examine if springtime subtropical marine Sc and SCT properties are in a statistical sense significantly influenced by different levels of complexity of the aerosol–cloud interaction parameterization (interactive versus non-interactive). We have also analyzed the impact of using low (~135 km), medium (~60 km) and high (~25 km) horizontal resolution. We chose the spring season of each hemisphere as this is when the regions are most cloudy and generally display the largest sensitivity to changing environmental conditions. All model versions use high-resolution sea surface temperature fields (HadISST2.2; Kennedy *et al.*, 2017) that are remapped to the respective model grid. In the non-interactive version of the aerosol–cloud model (EasyAerosol), prescribed monthly-averaged background aerosol optical properties and CDNCs were based on simulations using the interactive aerosol–cloud version of HadGEM3 (GLOMAP).

No significant change in the areal extent of the different cloud regimes along the four different SCT transects was found in any of the simulations. Significant, although small, changes in precipitation, liquid water and TOA SW CRE were found along the SCT transects and in all four marine Sc regions – both when changing the horizontal resolution and the aerosol–cloud interaction parameterization complexity. However, the impact on all-sky net SW TOA radiation was in general non-significant. Overall, the liquid water content was higher and precipitation rates were lower when higher resolution or non-interactive aerosols were used, in particular over the southern hemisphere.

Changing from low (135 km) to medium (60 km) horizontal resolution had the largest impact on the stratocumulus SW CRE, with significant mean seasonal and domain average differences up to 10 W m^{-2} over the Namibian marine Sc region (comparing MedRes-EA and LowRes-EA). Changing the resolution from medium to high (25-km) resolution resulted in smaller (about 1–2 W m^{-2}) but still significant differences in SW CRE (comparing HighRes-EA and MedRes-EA), indicating that the effect of changing horizontal model resolution may saturate at very high resolutions. A comparison with satellite-retrieved values of SW CRE showed that a higher liquid water path and higher SW CRE did not always improve the model performance. In this study, we have not examined the impact of changing the vertical resolution of the model which may result in a larger impact on the SCT and marine Sc properties (cf. e.g., Neubauer *et al.*, 2014).

While the difference in SW CRE changed monotonically and similarly over all regions and transects with increasing horizontal resolution, the difference was more complex when changing from non-interactive to interactive aerosols. Over the southern-hemisphere regions and transects, the higher liquid water content in MedRes-EA (non-interactive aerosols) than in MedRes-GLOMAP (interactive aerosols) resulted in a significantly more negative SW CRE of 2–6 W m^{-2}. Over the northern-hemisphere regions and transects, the change in liquid water was smaller and the higher CDNCs in MedRes-GLOMAP compared to MedRes-EA resulted in a higher (2–3 W m^{-2} more negative) SW CRE, or a non-significant change, when the interactive aerosol model version was used. We therefore conclude that a change in the complexity of the aerosol–cloud parameterization may significantly affect the TOA SW CRE, at least locally, but the sign and magnitude of the impact

will depend on the background level and relative change in liquid water as well as the absolute change in CDNC of the specific model version. Interestingly, the simulations with interactive aerosols generally brought the model closer to the satellite-retrieved values of the SW CRE compared to when using non-interactive aerosols. We note that the background CDNCs in the lower-complexity version of the aerosol–cloud model applied (EasyAerosol) were obtained using the same host model (HadGEM3) as in the high-complexity aerosol–cloud simulations. The differences obtained using non-interactive and interactive aerosols will most likely be larger if different host models are used for the different simulations, in particular if a fully coupled ocean–atmosphere GCM is applied where the location of major precipitation regions, such as the intertropical convergence zone, and subsequent wet scavenging of aerosols may be very different. This result lends support to the MACv2-SP protocol, which applies relative, rather than absolute, anomalies to model background CDNCs for the same reasons. Furthermore, in HadGEM3, the CDNCs used in the radiative and precipitation calculations are diagnostic; using a model with prognostic CDNCs may result in even larger differences between the interactive and non-interactive aerosol model (Yamaguchi *et al.*, 2017; Bulatovic *et al.*, 2019) and such comparisons would be interesting to conduct in the future.

AUTHOR CONTRIBUTIONS

Annica M. L. Ekman: Conceptualization; formal analysis; investigation; methodology; project administration; supervision; writing – original draft. **Eva Nygren:** Formal analysis; investigation; methodology; writing – review and editing. **Alejandro Baró Pérez:** Formal analysis; investigation; writing – review and editing. **Matthias Schwarz:** Formal analysis; investigation; writing – review and editing. **Gunilla Svensson:** Investigation; writing - review and editing. **Nicolas Bellouin:** Formal analysis; investigation, writing - review and editing.

ACKNOWLEDGEMENTS

This study was financially supported by the European Union's Horizon 2020 Research and Innovation Programme under grant agreement no. 641727 (PRIMAVERA). The authors greatly acknowledge the availability of HadGEM-GC31 output: HadGEM-GC31-LL (http://doi.org/10.22033/ESGF/CMIP6.1901), HadGEM3-GC31-MM (http://doi.org/10.22033/ESGF/CMIP6.1902), HadGEM3-GC31-HH (http://doi.org/10.22033/ESGF/CMIP6.445). The HadGEM-GC31 simulations with the GLOMAP aerosol module are available upon request. We would also like to acknowledge the obs4MIPs activity, a project initiated by the National Aeronautical and Space Administration (NASA) and U.S. Department of Energy (DOE), with governance provided by the World Climate Research Program's (WCRP) Data Advisory Council (WDAC). The AOD dataset (Levy *et al.*, 2009) used in this work was obtained from the obs4MIPs (https://esgf-node.llnl.gov/projects/obs4mips/) project hosted on the Earth System Grid Federation (https://esgf.llnl.gov) with special thanks to the MODIS science and instrument teams. We acknowledge the Global Precipitation Climatology Project and the NASA Langley Research Center for making their satellite data products available.

CONFLICT OF INTEREST

The authors declare no conflict of interest.

DATA AVAILABILITY STATEMENT

The authors gratefully acknowledge the availability of HadGEM3-GC3.1 output: HadGEM3-GC3.1-LL (http://doi.org/10.22033/ESGF/CMIP6.1901), HadGEM3-GC3.1-MM (http://doi.org/10.22033/ESGF/CMIP6.1902), HadGEM3-GC3.1-HH (http://doi.org/10.22033/ESGF/CMIP6.445). The HadGEM-GC3.1 simulations with the GLOMAP aerosol module are available upon request.

ORCID

Annica M. L. Ekman https://orcid.org/0000-0002-5940-2114
Gunilla Svensson https://orcid.org/0000-0001-9074-7623

REFERENCES

Abdul-Razzak, H. and Ghan, S.J. (2000) A parameterization of aerosol activation: 2. Multiple aerosol types. *Journal of Geophysical Research*, 105, 6837–6844. https://doi.org/10.1029/1999JD901161.

Abel, S.J. and Boutle, I.A. (2012) An improved representation of the raindrop size distribution for single-moment microphysics schemes. *Quarterly Journal of the Royal Meteorological Society*, 138, 2151–2162. https://doi.org/10.1002/qj.1949.

Abel, S.J. and Shipway, B.J. (2007) A comparison of cloud-resolving model simulations of trade wind cumulus with aircraft observations taken during RICO. *Quarterly Journal of the Royal Meteorological Society*, 133, 781–794. https://doi.org/10.1002/qj.55.

Adler, R., Wang, J.-J., Sapiano, M., Huffman, G., Chiu, L., Xie, P.P., Ferraro, R., Schneider, U., Becker, A., Bolvin, D., Nelkin, E., Gu, G. and NOAA CDR Program. (2016) Global precipitation climatology project (GPCP) climate data record (CDR), version 2.3 (monthly). *National Centers for Environmental Information*. https://doi.org/10.7289/V56971M6.

Adler, R.F., Sapiano, M., Huffman, G.J., Wang, J.-J., Gu, G., Bolvin, D., Chiu, L., Schneider, U., Becker, A., Nelkin, E., Xie, P., Ferraro,

R. and Shin, D.-B. (2018) The global precipitation climatology project (GPCP) monthly analysis (new version 2.3) and a review of 2017 global precipitation. *Atmosphere*, 9(4), 138. https://doi.org/10.3390/atmos9040138.

Albrecht, B.A., Bretherton, C.S., Johnson, D., Shubert, W.H. and Frisch, A.S. (1995) The Atlantic stratocumulus transition experiment—ASTEX. *Bulletin of the American Meteorological Society*, 76, 889–904.

Bellomo, K., Clement, A.C., Norris, J.R. and Soden, B.J. (2014) Observational and model estimates of cloud amount feedback over the Indian and Pacific oceans. *Journal of Climate*, 27, 925–940.

Bellouin, N., Mann, G.W., Woodhouse, M.T., Johnson, C., Carslaw, K.S. and Dalvi, M. (2013) Impact of the modal aerosol scheme GLOMAP-mode on aerosol forcing in the Hadley Centre global environmental model. *Atmospheric Chemistry and Physics*, 13, 3027–3044.

Bellouin, N., Rae, J., Jones, A., Johnson, C., Haywood, J. and Boucher, O. (2011) Aerosol forcing in the climate model Intercomparison project (CMIP5) simulations by HadGEM2-ES and the role of ammonium nitrate. *Journal of Geophysical Research*, 116, D20206. https://doi.org/10.1029/2011JD016074.

Blossey, P.N., Bretherton, C.S., Zhang, M., Cheng, A., Endo, S., Heus, T., Liu, Y., Lock, A.P., de Roode, S.R. and Xu, K.-M. (2013) Marine low cloud sensitivity to an idealized climate change: the CGILS LES intercomparison. *Journal of Advances in Modeling Earth Systems*, 5, 234–258. https://doi.org/10.1002/jame.20025.

Bony, S. and Dufresne, J.-L. (2005) Marine boundary layer clouds at the heart of cloud feedback uncertainties in climate models. *Geophysical Research Letters*, 32, L20806. https://doi.org/10.1029/2005GL023851.

Boutle, I.A., Eyre, J.E.J. and Lock, A.P. (2014a) Seamless stratocumulus simulation across the turbulent gray zone. *Monthly Weather Review*, 142, 1655–1668. https://doi.org/10.1175/MWR-D-13-00229.1.

Boutle, I.A., Abel, S.J., Hill, P.G. and Morcrette, C.J. (2014b) Spatial variability of liquid cloud and rain: observations and microphysical effects. *Quarterly Journal of the Royal Meteorological Society*, 140, 583–594. https://doi.org/10.1002/qj.2140.

Bulatovic, I., Ekman, A.M.L., Savre, J., Riipinen, I. and Leck, C. (2019) Aerosol indirect effects in marine stratocumulus: the importance of explicitly predicting cloud droplet activation. *Geophysical Research Letters*, 46, 3473–3481. https://doi.org/10.1029/2018GL081746.

Bretherton, C.S., Krueger, S.K., Wyant, M.C., Bechtold, P., Meijgaard, E.V., Stevens, B. and Teixeira, J. (1999) A GCSS boundary-layer cloud model intercomparison study of the first ASTEX Lagrangian experiment. *Boundary-Layer Meteorol.*, 93, 341–380.

Bretherton, C.S. and Wyant, M.C. (1997) Moisture transport, lower-tropospheric stability, and decoupling of cloud-topped boundary layers. *Journal of the Atmospheric Sciences*, 54, 148–167.

Bretherton, C.S. (2015) Insights into low-latitude cloud feedbacks from high-resolution models. *Philosophical Transactions of the Royal Society A*, 373, 20140415. https://doi.org/10.1098/rsta.2014.0415.

Brient, F. and Bony, S. (2013) Interpretation of the positive low-cloud feedback predicted by a climate model under global warming. *Climate Dynamics*, 40, 2415–2431.

Brown, A.R., Beare, R.J., Edwards, J.M., Lock, A.P., Keogh, S.J., Milton, S.F. and Walters, D.N. (2008) Upgrades to the boundary-layer scheme in the met Office numerical weather prediction model. *Boundary-Layer Meteorology*, 128, 117–132. https://doi.org/10.1007/s10546-008-9275-0.

Ceppi, P., Brient, F., Zelinka, M.D. and Hartmann, D.L. (2017) Cloud feedback mechanisms and their representation in global climate models. *WIREs Climate Change*, 8, e465. https://doi.org/10.1002/wcc.465.

Chen, G. and Wang, W.-C. (2016) Aerosol–stratocumulus–radiation interactions over the Southeast Pacific: implications to the underlying Air–Sea coupling. *Journal of the Atmospheric Sciences*, 73, 2759–2771. https://doi.org/10.1175/JAS-D-15-0277.1.

Clement, A.C., Burgman, R. and Norris, J.R. (2009) Observational and model evidence for positive low-level cloud feedback. *Science*, 325, 460–464.

Loeb, N.G., Doelling, D.R., Wang, H., Su, W., Nguyen, C., Corbett, J.G., Liang, L., Mitrescu, C., Rose, F.G. and Kato, S. (2018) Clouds and the Earth's radiant energy system (CERES) energy balanced and filled (EBAF) top-of-atmosphere (TOA) Edition-4.0 data product. *Journal of Climate*, 31, 895–918. https://doi.org/10.1175/JCLI-D-17-0208.1.

Eastman, R., Warren, S.G. and Hahn, C.J. (2011) Variations in cloud cover and cloud types over the ocean from surface observations, 1954–2008. *Journal of Climate*, 24, 5914–5934.

Edwards, J.M. and Slingo, A. (1996) Studies with a flexible new radiation code. I: choosing a configuration for a large-scale model. *Quarterly Journal of the Royal Meteorological Society*, 122, 689–719.

Ekman, A.M.L. (2014) Do sophisticated parameterizations of aerosol-cloud interactions in CMIP5 models improve the representation of recent observed temperature trends? *Journal of Geophysical Research*, 119, 817–832. https://doi.org/10.1002/2013JD020511.

Elsaesser, G.S., O'Dell, C.W., Lebsock, M.D., Bennartz, R. and Greenwald, T.J. (2017) The multi-sensor advanced climatology of liquid water path (MAC-LWP). *Journal of Climate*, 30(24), 10193–10210. https://doi.org/10.1175/JCLI-D-16-0902.1.

Hahn, C.J. and Warren, S.G. (2007) *A Gridded Climatology of Clouds over Land (1971–96) and Ocean (1954–97) from Surface Observations Worldwide*. Oak Ridge, TN: Numeric Data Package NDP-026EORNL/CDIAC-153, CDIAC, Department of Energy.

Hersbach, H., Bell, B., Berrisford, P., Hirahara, S., Horanyi, A., Munoz-Sabater, J., Nicolas, J., Peubey, C., Radu, R., Schepers, D., Simmons, A., Soci, C., Abdallaa, S., Abellan, X., Balsamo, G., Bechtold, P., Biavati, G., Bidlot, J., Bonavita, M., DeChiara, G., Dahlgren, P., Dee, D., Diamantakis, M., Dragani, R., Flemming, J., Forbes, R., Fuentes, M., Geer, A., Haimberger, L., Healy, S., Hogan, R.J., Holm, E., Janiskova, M., Keeley, S., Laloyaux, P., Lopez, P., Radnoti, G., de Rosnay, P., Rozum, I., Vamborg, F., Villaume, S. and Thepaut, J.N. (2020) The ERA5 global reanalysis. *Quarterly Journal of the Royal Meteorological Society*, 146(730), 1999–2049. https://doi.org/10.1002/qj.3803.

Hoesly, R.M., Smith, S.J., Feng, L., Klimont, Z., Janssens Maenhout, G., Pitkanen, T., Seibert, J.J., Vu, L., Andres, R.J., Bolt, R.M., Bond, T.C., Dawidowski, L., Kholod, N., Kurokawa, J.-I., Li, M., Liu, L., Lu, Z., Moura, M.C.P., O'Rourke, P.R. and Zhang, Q. (2018) Historical (1750–2014) anthropogenic emissions of reactive gases and aerosols from the community emissions data system (CEDS). *Geoscientific Model Development*, 11, 369–408. https://doi.org/10.5194/gmd-11-369-2018.

Karlsson, J., Svensson, G. and Rodhe, H. (2008) Cloud radiative forcing of subtropical low level clouds in global models. *Climate Dynamics*, 30, 779–788. https://doi.org/10.1007/s00382-007-0322-1.

Kennedy, J., Titchner, H., Rayner, N. and Roberts, M. (2017) input4MIPs.MOHC.SSTs and SeaIce.HighResMIP. MOHCHadISST-2-2-0-0-0. Version 20170505, Earth System Grid Federation. https://doi.org/10.22033/ESGF/input4MIPs.1221.

Khairoutdinov, M. and Kogan, Y. (2000) A new cloud physics parameterization in a large-eddy simulation model of marine stratocumulus. *Monthly Weather Review*, 128, 229–243. https://doi.org/10.1175/1520-0493(2000)128<0229:ANCPPI>2.0.CO;2.

Klein, S.A. and Hartmann, D.L. (1993) The seasonal cycle of low stratiform clouds. *Journal of Climate*, 6, 1587–1606. https://doi.org/10.1175/1520-0442(1993)006<1587:TSCOLS>2.0.CO;2.

Kodros, J.K. and Pierce, J.R. (2017) Important global and regional differences in aerosol cloud-albedo effect estimates between simulations with and without prognostic aerosol microphysics. *Journal of Geophysical Research*, 122, 4003–4018. https://doi.org/10.1002/2016JD025886.

Konsta, D., Dufresne, J.-L., Chepfer, H., Vial, J., Koshiro, T., Kawai, H., Bodas-Salcedo, A., Roehrig, R., Watanabe, M. and Ogura, T. (2022) Low-level marine tropical clouds in six CMIP6 models are too few, too bright but also too compact and too homogeneous. *Geophysical Research Letters*, 49, e2021GL097593. https://doi.org/10.1029/2021GL097593.

Kuhlbrodt, T., Jones, C.G., Sellar, A., Storkey, D., Blockley, E., Stringer, M., Hill, R., Graham, T., Ridley, J., Blaker, A., Calvert, D., Copsey, D., Ellis, R., Hewitt, H., Hyder, P., Ineson, S., Mulcahy, J., Siahaan, A. and Walton, J. (2018) The low-resolution version of HadGEM3 GC3.1: development and evaluation for global climate. *Journal of Advances in Modeling Earth Systems*, 10, 2865–2888. https://doi.org/10.1029/2018MS001370.

Levy, R.C., Remer, L.A., Tanré, D., Mattoo, S. and Kaufman, Y.J. (2009) Algorithm for Remote Sensing of Tropospheric Aerosol Over Dark Targets from MODIS. Collections 005 and 051. Revision 2. Available from http://modisatmos.gsfc.nasa.gov/MOD04_L2/atbd.html.

Lock, A.P. (2001) The numerical representation of entrainment in parametrizations of boundary layer turbulent mixing. *Monthly Weather Review*, 129, 1148–1163. https://doi.org/10.1175/1520-0493(2001)129<1148:TNROEI>2.0.CO;2.

Lock, A.P., Brown, A.R., Bush, M.R., Martin, G.M. and Smith, R.N.B. (2000) A new boundary layer mixing scheme. Part I: scheme description and single-column model tests. *Monthly Weather Review*, 128, 3187–3199. https://doi.org/10.1175/1520-0493(2000)128<3187:ANBLMS>2.0.CO;2.

Mann, G.W., Carslaw, K.S., Spracklen, D.V., Ridley, D.A., Manktelow, P.T., Chipperfield, M.P., Pickering, S.J. and Johnson, C.E. (2010) Description and evaluation of GLOMAP-mode: a modal global aerosol microphysics model for the UKCA composition-climate model. *Geoscientific Model Development*, 3, 519–551. https://doi.org/10.5194/gmd-3-519-2010.

Martin, G.M., Johnson, D.W. and Spice, A. (1994) The measurement and parameterization of effective radius of droplets in warm stratiform clouds. *Journal of the Atmospheric Sciences*, 51, 1823–1842.

McCoy, D.T., Eastman, R., Hartmann, D.L. and Wood, R. (2017) The change in low cloud cover in a warmed climate inferred from AIRS, MODIS, and ERA-interim. *Journal of Climate*, 30, 3609–3620.

Menary, M.B., Kuhlbrodt, T., Ridley, J., Andrews, M.B., Dimdore-Miles, O.B., Deshayes, J., Eade, R., Gray, L., Ineson, S., Mignot, J., Roberts, C.D., Robson, J., Wood, R.A. and Xavier, P. (2018) Preindustrial control simulations with HadGEM3-GC3.1 for CMIP6. *Journal of Advances in Modeling Earth Systems*, 10, 3049–3075. https://doi.org/10.1029/2018MS001495.

Nam, C., Bony, S., Dufresne, J.-L. and Chepfer, H. (2012) The 'too few, too bright' tropical low-cloud problem in CMIP5 models. *Geophysical Research Letters*, 39, L21801.

Neggers, R.A.J., Ackerman, A.S., Angevine, W.M., Bazile, E., Beau, I., Blossey, P.N., Boutle, I.A., de Bruijn, C., Cheng, A., van der Dussen, J., Fletcher, J., Dal Gesso, S., Jam, A., Kawai, H., Cheedela, S.K., Larson, V.E., Lefebvre, M.-P., Lock, A.P., Meyer, N.R., de Roode, S.R., de Rooy, W., Sandu, I., Xiao, H. and Xu, K.-M. (2017) Single-column model simulations of subtropical marine boundary-layer cloud transitions under weakening inversions. *JAMES*, 9, 2385–2412. https://doi.org/10.1002/2017MS001064.

Neubauer, D., Lohmann, U., Hoose, C., Hoose, C. and Frontoso, M.G. (2014) Impact of the representation of marine stratocumulus clouds on the anthropogenic aerosol effect. *Atmospheric Chemistry and Physics*, 14, 11997–12022.

Norris, J. (1998) Low cloud type over the ocean from surface observations. Part II: geographical and seasonal variations. *Journal of the Atmospheric Sciences*, 11, 383–403.

Phillips, T.J., Corsetti, L.C. and Grotch, S.L. (1995) The impact of horizontal resolution on moist processes in the ECMWF model. *Climate Dynamics*, 11(85), 102.

Rasch, P.J., Xie, S., Ma, P.-L., Lin, W., Wang, H., Tang, Q., Burrows, S.M., Caldwell, P., Zhang, K., Easter, R.C., Cameron-Smith, P., Singh, B., Wan, H., Golaz, J.C., Harrop, B.E., Roesler, E., Bacmeister, J., Larson, V.E., Evans, K.J., Qian, Y., Taylor, M., Leung, L.R., Zhang, Y., Brent, L., Branstetter, M., Hannay, C., Mahajan, S., Mametjanov, A., Neale, R., Richter, J.H., Yoon, J.H., Zender, C.S., Bader, D., Flanner, M., Foucar, J.G., Jacob, R., Keen, N., Klein, S.A., Liu, X., Salinger, A.G., Shrivastava, M. and Yang, Y. (2019) An overview of the atmospheric component of the energy Exascale earth system model. *Journal of Advances in Modeling Earth Systems*, 11, 2377–2411. https://doi.org/10.1029/2019MS001629.

Roberts, M.J., Baker, A., Blockley, E.W., Calvert, D., Coward, A., Hewitt, H.T., Jackson, L.C., Kuhlbrodt, T., Mathiot, P., Roberts, C.D., Scheimann, R., Seddon, J., Vannière, B. and Vidale, P.L. (2019) Description of the resolution hierarchy of the global coupled HadGEM3-GC3.1 model as used in CMIP6 HighResMIP experiments. *Geoscientific Model Development*, 12, 4999–5028.

Sandu, I., Stevens, B. and Pincus, R. (2010) On the transitions in marine boundary layer cloudiness. *Atmospheric Chemistry and Physics*, 10, 2377–2391.

Sandu, I. and Stevens, B. (2011) On the factors modulating the stratocumulus to cumulus transitions. *Journal of the Atmospheric Sciences*, 68, 1865–1881.

Schneider, T., Kaul, C.M. and Pressel, K.G. (2019) Possible climate transitions from breakup of stratocumulus decks under greenhouse warming. *Nature Geoscience*, 12, 163–167.

Slingo, A. (1990) Sensitivity of the Earth's radiation budget to changes in low clouds. *Nature*, 343, 49–51.

Soden, B.J. and Vecchi, G.A. (2011) The vertical distribution of cloud feedback in coupled ocean-atmosphere models. *Geophysical Research Letters*, 38, L12704. https://doi.org/10.1029/2011GL047632.

Stevens, B., Fiedler, S., Kinne, S., Peters, K., Rast, S., Müsse, J., Smith, S.J. and Mauritsen, T. (2017) MACv2-SP: a parameterization of anthropogenic aerosol optical properties and an associated Twomey effect for use in CMIP6. *Geoscientific Model Development*, 10, 433–452.

Svensson, G., Tjernström, M. and Koracin, D. (2000) The sensitivity of a stratocumulus transition: model simulations of the ASTEX first Lagrangian. *Bound-Layer Meteorology*, 95, 57–90.

Teixeira, J., Cardoso, S., Bonazzola, M., Cole, J.N., DelGenio, A.D., DeMott, C., Franklin, A., Hannay, C., Jakob, C., Jiao, Y., Karlsson, J., Kitagawa, H., Koehler, M., Kuwano-Yoshida, A., LeDrian, C., Lock, A., Miller, M., Marquet, P., Martins, J., Mechoso, C.R., Meijgaard, E.V., Meinke, I., Miranda, P., Mironov, D., Neggers, R., Pan, H.L., Randall, D.A., Rasch, P.J., Rockel, B., Rossow, W.B., Ritter, B., Siebesma, A.P., Soares, P., Turk, F.J., Vaillancourt, P., Von Engeln, A. and Zhao, M. (2011) Tropical and subtropical cloud transitions in weather and climate prediction models: the GCSS/WGNE Pacific cross-section Intercomparison (GPCI). *Journal of Climate*, 24, 5223–5256. https://doi.org/10.1175/2011JCLI3672.1.

Terai, C.R., Pritchard, M.S., Blossey, P. and Bretherton, C.S. (2020) The impact of resolving subkilometer processes on aerosol-cloud interactions of low-level clouds in global model simulations. *Journal of Advances in Modeling Earth Systems*, 12, e2020MS002274. https://doi.org/10.1029/2020MS002274.

Thomas, M.A., Devasthale, A., Koenigk, T., Wyser, K., Roberts, M., Roberts, C. and Lohmann, K. (2019) A statistical and process-oriented evaluation of cloud radiative effects in high-resolution global models. *Geoscientific Model Development*, 12, 1679–1702. https://doi.org/10.5194/gmd-12-1679-2019.

Vial, J., Bony, S., Dufresne, J.-L. and Roehrig, R. (2016) Coupling between lower-tropospheric convective mixing and low-level clouds: physical mechanisms and dependence on convection scheme. *Journal of Advances in Modeling Earth Systems*, 8, 1892–1911.

Walters, D., Baran, A.J., Boutle, I., Brooks, M., Earnshaw, P., Edwards, J., Furtado, K., Hill, P., Lock, A., Manners, J., Morcrette, C., Mulcahy, J., Sanchez, C., Smith, C., Stratton, R., Tennant, W., Tomassini, L., van Weverberg, K., Vosper, S., Willett, M., Browse, J., Bushell, A., Carslaw, K., Dalvi, M., Essery, R., Gedney, N., Hardiman, S., Johnson, B., Johnson, C., Jones, A., Jones, C., Mann, G., Milton, S., Rumbold, H., Sellar, A., Ujiie, M., Whitall, M., Williams, K. and Zerroukat, M. (2019) The met Office unified model global atmosphere 7.0/7.1 and JULES global land 7.0 configurations. *Geoscientific Model Development*, 12, 1909–1963. https://doi.org/10.5194/gmd-12-1909-2019.

West, R.E.L., Stier, P., Jones, A., Johnson, C.E., Mann, G.W., Bellouin, N., Partridge, D.G. and Kipling, Z. (2014) The importance of vertical velocity variability for estimates of the indirect aerosol effects. *Atmospheric Chemistry and Physics*, 14, 6369–6393.

Wilcox, L.J., Highwood, E.J. and Dunstone, N.J. (2013) The influence of anthropogenic aerosol on multi-decadal variations of historical global climate. *Environmental Research Letters*, 8(2), 024033. https://doi.org/10.1088/1748-9326/8/2/024033.

Williams, K.D., Copsey, D., Blockley, E.W., Bodas-Salcedo, A., Calvert, D., Comer, R. and Xavier, P.K. (2017) The met Office global coupled model 3.0 and 3.1 (GC3.0 and GC3.1) configurations. *Journal of Advances in Modeling Earth Systems*, 10, 357–380. https://doi.org/10.1002/2017MS001115.

Wilson, D.R., Bushell, A.C., Kerr-Munslow, A.M., Price, J.D. and Morcrette, C.J. (2008) PC2: a prognostic cloud fraction and condensation scheme. I: scheme description. *Quarterly Journal of the Royal Meteorological Society*, 134, 2093–2107.

Wood, R. (2012) Stratocumulus Clouds. *Monthly Weather Review*, 140, 2373–2423.

Wood, R. and Bretherton, C.S. (2004) Boundary layer depth, entrainment, and decoupling in the cloud-capped subtropical and tropical marine boundary layer. *Journal of Climate*, 17, 3576–3588.

Xie, S., Lin, W., Rasch, P.J., Ma, P.-L., Neale, R., Larson, V.E., Qian, Y., Bogenschutz, P.A., Caldwell, P., Cameron-Smith, P., Golaz, J.C., Mahajan, S., Singh, B., Tang, Q., Wang, H., Yoon, J.H., Zhang, K. and Zhang, Y. (2018) Understanding cloud and convective characteristics in version 1 of the E3SM atmosphere model. *Journal of Advances in Modeling Earth Systems*, 10, 2618–2644. https://doi.org/10.1029/2018MS001350.

Yamaguchi, T., Feingold, G. and Kazil, J. (2017) Stratocumulus to cumulus transition by drizzle. *Journal of Advances in Modeling Earth Systems*, 9, 2333–2349. https://doi.org/10.1002/2017MS001104.

Zhang, M., Bretherton, C.S., Blossey, P.N., Austin, P.H., Bacmeister, J.T., Bony, S., Brient, F., Cheedela, S.K., Cheng, A., Del Genio, A.D., et al. (2013) CGILS: results from the first phase of an international project to understand the physical mechanisms of low cloud feedbacks in single column models. *Journal of Advances in Modeling Earth Systems*, 5, 826–842.

How to cite this article: Ekman, A.M.L., Nygren, E., Pérez, A.B., Schwarz, M., Svensson, G. & Bellouin, N. (2023) Influence of horizontal resolution and complexity of aerosol–cloud interactions on marine stratocumulus and stratocumulus-to-cumulus transition in HadGEM3-GC3.1. *Quarterly Journal of the Royal Meteorological Society*, 1–18. Available from: https://doi.org/10.1002/qj.4494

APPENDIX A

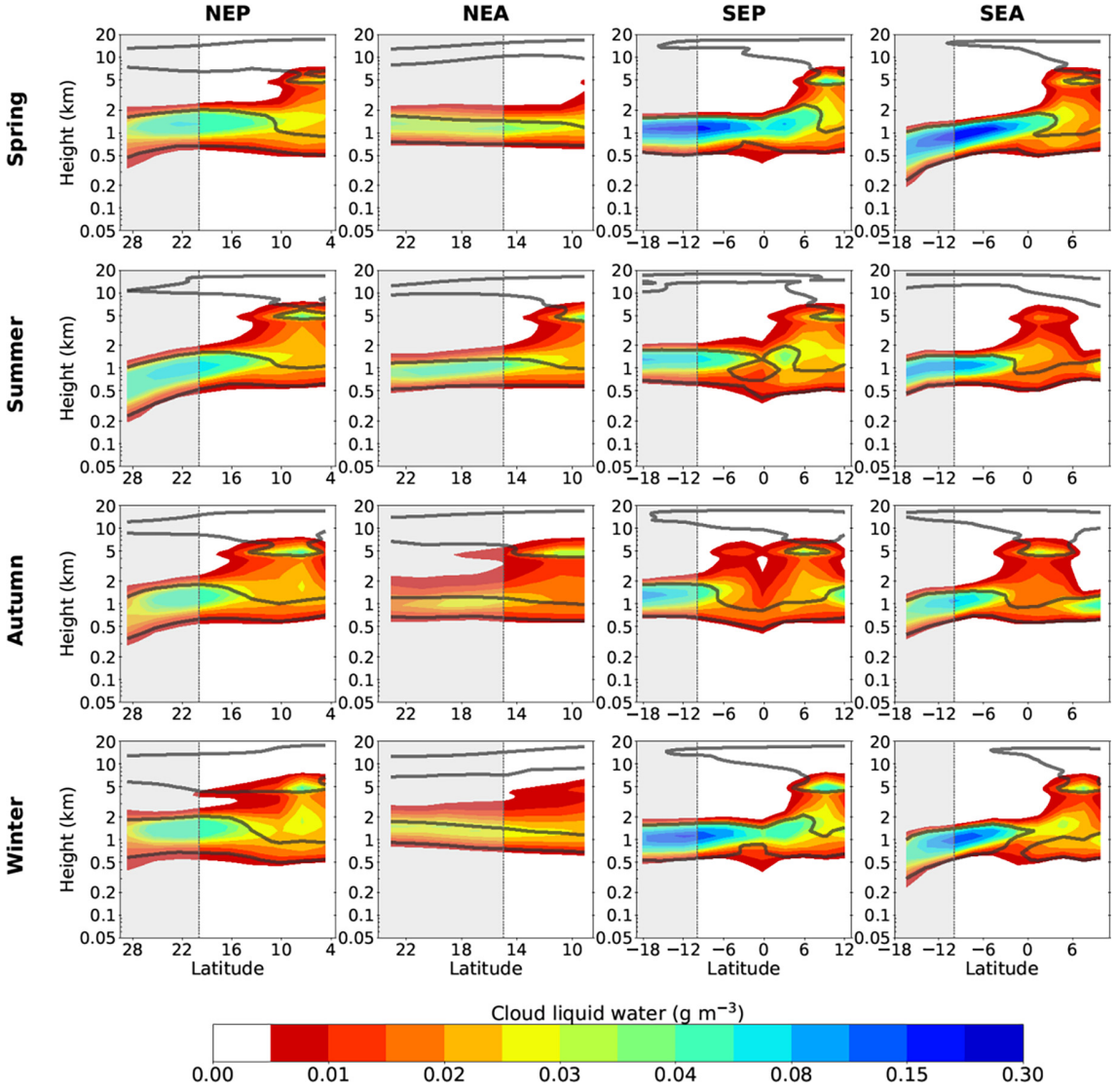

FIGURE A1 Mean vertical cross-section of cloud liquid water (colors) together with the mean cloud fraction (contours) for all transects (left to right: NEP, NEA, SEP, SEA) for all seasons in each hemisphere (top to bottom: Spring, Summer, Fall, Winter) for the MedRes-EA version of HadGEM3. Isolines denote 5%, 10% and 25% cloud fractions. The stratocumulus regions are marked with shaded boxes [Colour figure can be viewed at wileyonlinelibrary.com]